Int. J. Heat Mass Transfer. Vol. 34, No. 4/5, pp. 1027–1041, 1991
Printed in Great Britain

0017–9310/91 $3.00 + 0.00

An experimental–computational investigation of the heat transfer in mechanical face seals

J. C. DOANE
6023 Navigation Blvd., Houston, TX 77253, U.S.A.

and

T. A. MYRUM and J. E. BEARD
Mechanical Engineering Department, Louisiana State University, Baton Rouge, LA 70803, U.S.A.

(*Received* 6 *February* 1990 *and in final form* 25 *May* 1990)

Abstract—Experimental measurements are combined with computations to obtain local and average heat transfer information for the face of the seat of a mechanical face seal used to seal water for shaft speeds of 1500, 2500, and 3000 rpm. Local and average Nusselt number results are also obtained (to within ±20%) for the water-wetted circumference of the seat. The average Nusselt numbers for the two largest shaft speeds are accurately predicted using the standard equations for turbulent flat plate flow to compute the Nusselt numbers for the rotating portion and setting them equal to those for the seat.

INTRODUCTION

MECHANICAL face seals are commonly used in pumps, turbines, agitators, mixers, and other types of rotating equipment to prevent leakage. These seals are subject to leakage and premature failure. The impact of seal failure is both an economic one, in terms of seal replacement and lost production, and an environmental one, in terms of the leakage of toxic substances into the environment. Therefore, the importance of seal design, especially during a time when public consciousness is turning toward environmental issues, cannot be overemphasized.

Figure 1 shows a cross-sectional view of the seal used in this study. It is a production-type seal manufactured by John Crane Inc, Morton Grove, Illinois. The basic idea behind the operation of a face seal is to reduce the leakage path between the rotating seal face and the stationary seat face. This is accomplished by using perfectly flat face surfaces (the surfaces are lapped to within 0.56 μm) and using the sealed fluid pressure along with a spring force to press the seal face against the seat face.

Typically, but not always, a fine liquid film a few micrometers thick separates the two faces. At the present time, the morphology of this film is a topic of ongoing research. Reference [1] measured the average thickness of a liquid film and found it to depend on the shaft speed and the type of sealed fluid being used. Typical values ranged from 1 to 14 μm. It should be mentioned that in some instances, local or global vaporization may occur in the film.

The amount of leakage and wear in mechanical face seals depends upon the shape of the interface separating the seal and seat faces. Since both faces are lapped flat prior to installation, the initial shape of the interface is uniform across the face. However, during operation, the faces undergo considerable distortion due to the sealant pressure and thermal effects [2]. Reference [2] also pointed out that pressure induced distortions can easily be controlled, but the thermal effects are significant and often hard to predict. Such distortions lead to excessive leakage and premature seal failure. This is particularly important when the sealed fluid is toxic or highly volatile. In order to accurately predict the thermal distortion, via the seal temperature distribution, knowledge of the heat transfer characteristics of seals is essential.

Currently, the temperature distributions in the seal and seat cross-sections are determined from two-dimensional conduction models for the seal and seat using either finite difference, finite element, or boundary integral methods. In all of these studies, the boundaries exposed to the sealed fluid (liquid) are treated as convective boundaries with constant convection coefficients, and the boundaries exposed to air or contacted by 'O' rings are treated as essentially adiabatic. A variety of conditions are used for the seal–seat interface.

The main sources of discrepancy among the various models are the values of the heat transfer coefficients for the surfaces exposed to the sealed fluid and the boundary conditions for the seal–seat interface. In ref. [2], the temperature distribution in the rotating seal was determined from the boundary integral method using average Nusselt numbers for a shaft rotating in an annulus and a uniform temperature distribution at the interface. Finite differences were used in ref. [3] to compute the temperature distributions in the seal and seat. The average Nusselt number for the outer rotating surface of the seal was obtained from experiments on horizontal cylinders rotating in oil, while the

NOMENCLATURE

A_r	surface area of rotating seal face, $\pi(r_o^2 - r_i^2)$ [m^2]	Q_z	average heat transfer for region of seat face corresponding to the seal face [W]
A_z	wetted surface area of outer radial seat surface, $2\pi R_o \hat{z}$ [m^2]	q_z	heat at flux at seat face [W m^{-2}]
c_w	constant-pressure specific heat of water, 4.178 kJ kg^{-1} K^{-1}	r	radial coordinate
h	local heat transfer coefficient, equation (6)	r_i	inner radius of seal (2.03 cm)
k_s	seat thermal conductivity, equation (3)	R_o	outer radius of seat (2.69 cm)
k_w	water thermal conductivity at $(T_s(z) + T_r)/2$ [W m^{-1} K^{-1}]	r_o	outer radius of seal (2.63 cm)
m	mass flow rate in system, 0.048 kg s^{-1}	$T(r)$	seat face temperature [°C]
Nu	local Nusselt number, equation (7)	$T(r, z)$	cross-sectional temperature in seat
Nu_{AV}	average Nusselt number, equation (9)	T_{in}	temperature at test chamber inlet, 30.7 °C
Q_{gen}	total heat generated at seal/seat interface, equation (11)	T_{out}	temperature at test chamber outlet [°C]
Q_r	average heat transfer for wetted portion of outer radial surface of seat [W]	$T_s(z)$	temperature at outer radial surface of seat [°C]
q_r	heat flux at wetted outer radial surface of seat [W m^{-2}]	T_r	ambient temperature, $(T_{in} + T_{out})/2$
		ΔT	average temperature difference, equation (10) [°C]
		z	axial coordinate
		$\hat{z}$	distance that the seat protruded into the sealed water (0.15 cm).

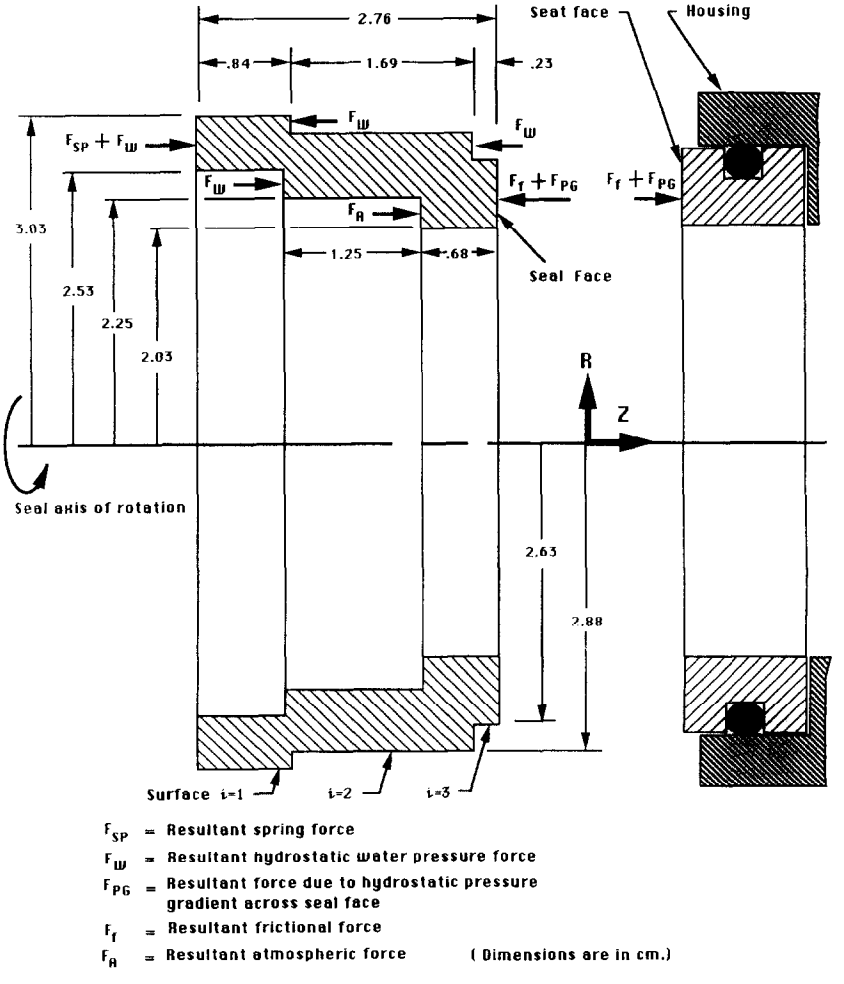

FIG. 1. Cross-sectional view of the rotating seal and fixed seat.

Dittus–Boelter equation was used to estimate the Nusselt number for the wetted portion of the outer radial seat surface. The interface boundary condition was determined by assuming a particular heat flux distribution (based on Couette flow at the interface) and iterating until the heat flux profile stopped changing.

Buck [4] performed analytical calculations based upon heat transfer efficiencies (similar to fin efficiencies). In the calculations, uniform heat flux distributions were assumed for the seal–seat interface, and the average Nusselt number for the wetted outer surface of the rotating seal was determined from the standard correlations for flow past a flat plate [5]. The Nusselt number for the wetted portion of the outer radial seat surface was set equal to that of the rotating seal.

It is apparent from the foregoing that there are a number of different methods being used to estimate the average Nusselt numbers for the wetted surfaces of the seal and seat. Therefore, measurements of the Nusselt numbers obtained from tests involving actual mechanical seals are desperately needed.

As for the thermal boundary condition at the interface, ref. [2] measured the temperatures near the face of the seat, using thermocouples, at radial locations corresponding to the inner and outer radii of the seal. Mineral oil was the sealed fluid. Two pairs of thermocouples were used to measure the temperature gradients in the seat at radial locations corresponding to the inner and outer radii of the seal in ref. [6] for water. In ref. [7], a rotating quartz seal was used to facilitate temperature measurements using an infrared pyrometer. This yielded the interface temperature profile for a variety of shaft speeds during start-up and steady-state operation. Water and 10W motor oil were the sealed fluids.

The present research is the result of a combined computational and experimental program performed to study the heat transfer for a 66% balanced mechanical face seal used to seal water, where the balance is the surface area acted on by F_w in the positive z-direction (see Fig. 1) minus the surface area acted on by F_w in the negative direction divided by the area of the seal face. The experimental setup consisted of a seal tester built specially to test production-type seals (see Figs. 2(a) and (b)). Measurements of the temperatures at various locations in the stationary seat portion comprised the experimental portion of the research. These temperatures were then used as the thermal boundary conditions in a finite difference solution of the two-dimensional, steady-state heat conduction in the seat. The resulting temperature distribution was used to back calculate the temperatures at the inner and outer radial surfaces of the seat.

Experiments and computations were performed for parametric variations of the shaft speed. Three different rotational speeds were considered during the research: 1500, 2500, and 3000 rpm. The results obtained at the various rotational speeds include: the temperature distribution across the seat face, cross-sectional isotherm maps, local and average heat transfer results for the seat face, and local and average Nusselt numbers for the portion of the outer radial seat surface wetted by the sealed water. At the largest rotational speed, the average heat transfer for the seal was determined.

EXPERIMENTAL APPARATUS

The experimental apparatus consisted of the seal tester, the water circulating loop and the instrumentation. Figure 2(a) shows a schematic of the apparatus.

The rotating portion consisted of a spring-loaded carbon seal insert (see Fig. 1) mounted in a stainless steel retainer. Eight identical helical springs evenly spaced around the base of the retainer provided the spring loading. The rotating portion was attached to a rotating shaft with one end of the shaft in the sealed test chamber (see Fig. 2(b)).

The bearing pairs used to support the shaft were outside the test chamber, thus enabling the mechanical face seal to be the only rotating component inside the test chamber. The rotating shaft was supported so the reaction forces on the drive pulley would not cause misalignment between the seal face and the seat. A variable speed motor capable of speeds ranging from 900 to 3000 rpm was used to drive the shaft.

The seat was made of 304 stainless steel and was contained in a counter bore in the mounting plate. This counter bore provided the same 0.15 cm protrusion of the seat into the sealed fluid as is present in most mechanical face seal applications. The 'O'-ring, was used to eliminate extraneous leakage.

Since the seat was attached directly to the rotating shaft, alignment was provided so the axis of rotation was perpendicular to the seat face. A dial indicator was used to insure perpendicularity to within 12.7 μm at the edge of the seat.

The circulating loop that delivers the water to the test chamber had a 140 liter tank kept at a constant temperature with a Lauda B-1 controller/circulator capable of maintaining the bath temperature within ± 0.1°C.

The pressure of the fluid circulating through the test chamber was maintained using a pump and pressure valve, which was located on the outlet side of the test chamber. The maximum variation of pressure was 2.5% of its mean value.

TEMPERATURE MEASUREMENT

Chromel and constantan thermocouples (0.0127 cm diameter) with a 0.0076 cm thick coating of Teflon insulation were used for all temperature measurements. These thermocouples have a sensitivity of about 62 μV °C^{-1}. The total number of thermocouples used depended on the particular seat being

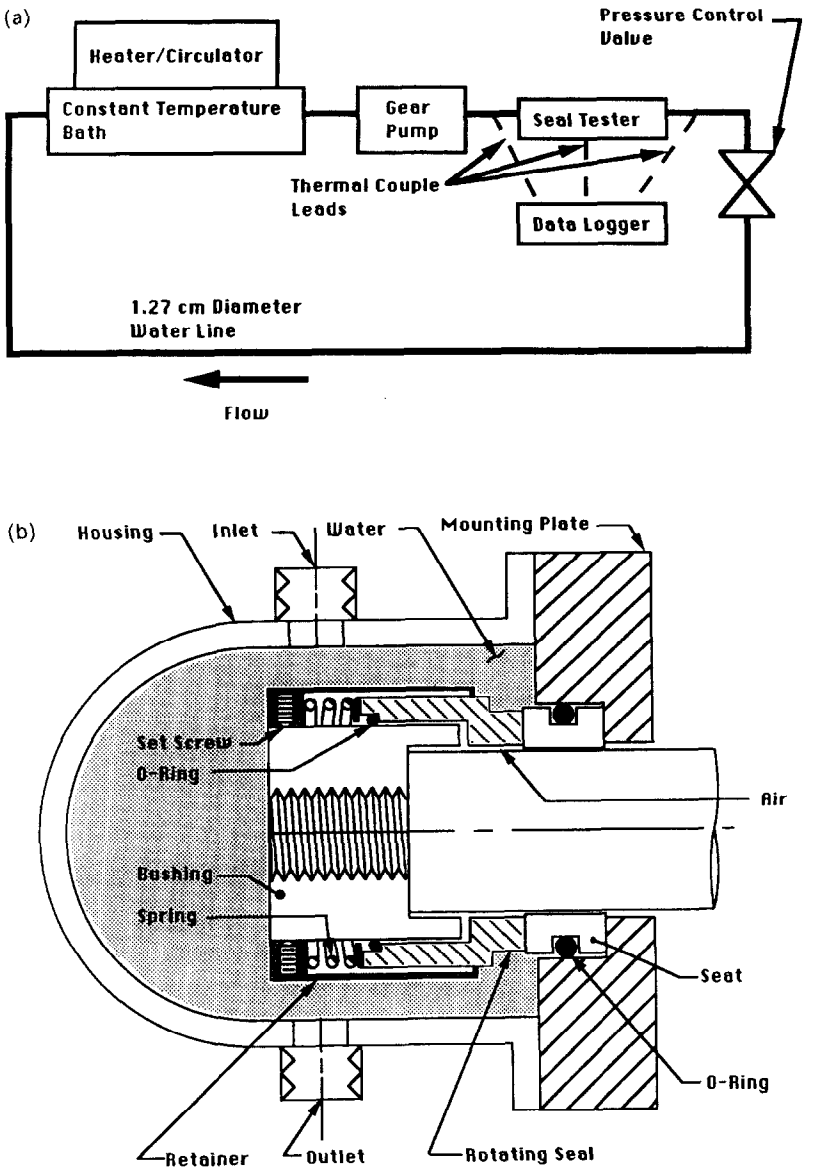

FIG. 2. Schematic of the apparatus and the seal test chamber: (a) schematic of apparatus; (b) test chamber and seal assembly.

used. However, three thermocouples were common to all of the data runs. They are the following: one for the ice point reference junction, one to measure the fluid temperature at the inlet to the test chamber, and one to measure the fluid temperature at the outlet of the test chamber. Thermowells were used to locate the thermocouples in the center of the flow passages near the inlet and the outlet. Although the thermowells were located as close as possible to the test chamber, the region between the thermowells and the test chamber was insulated to prevent heat transfer.

To determine if a two-dimensional model could be used, it was necessary to measure the circumferential temperature and compare its gradients to those in the radial and axial directions. This was accomplished by using three identical seats: one for the measurement of the circumferential distribution, one for the axial distribution, and one for the radial distribution. The basic seat dimensions are shown in Fig. 3(a).

In order to measure the circumferential distribution, eight thermocouples were equally spaced on a 2.34 cm base circle and were located 0.0127 cm from the seat face.

The seat used to measure the temperature in the axial direction had five thermocouples equally spaced 5 deg apart on a 2.34 cm base circle. They were located at the following distances from the face of the seat: 0.028, 0.061, 0.135, 0.264, and 0.028 cm. The two thermocouples located at the same depth (0.028 cm) were used to monitor possible angular temperature

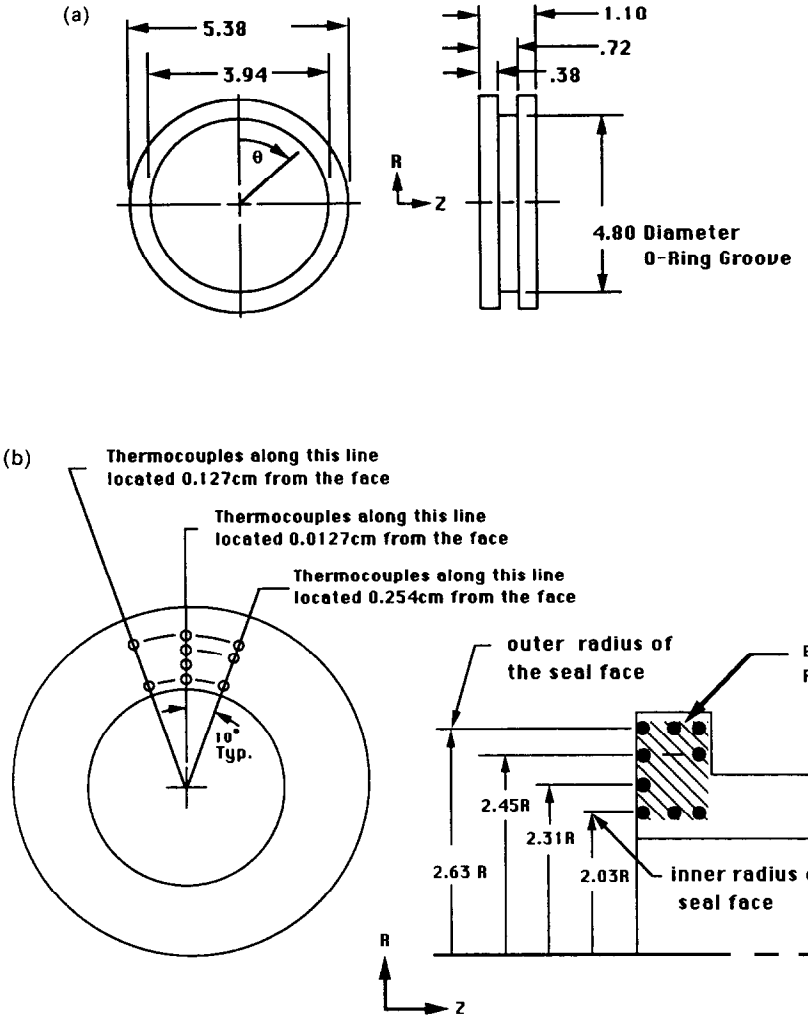

FIG. 3. Basic seal dimensions (cm) and thermocouple locations for boundary measurements: (a) basic seat dimensions; (b) thermocouple locations.

gradients. The temperature difference between these two thermocouples was typically less than 0.11°C in 20 deg of angular displacement (i.e. over a 0.82 cm arc length). It was found that the axial temperature gradient was at least 28 times larger than the circumferential temperature gradient. This suggested that the temperature gradients caused by the angular location of the thermocouples could be safely neglected.

The seat shown in Fig. 3(b) was used to measure the temperature in the radial direction. These thermocouples also provided the boundary conditions that were used to calculate the temperature distribution in the seat. Four thermocouples were placed as close to the seat face as possible (0.0127 cm) at the following radii: 2.03, 2.31, 2.45, and 2.63 cm. The radial temperature gradient was found to be at least 20 times greater than the circumferential gradient.

Since it was determined that the angular position of the thermocouples had a negligible effect on the measured temperature (<0.11°C), the thermocouples were located at different angular positions to facilitate the experimental measurement of the boundary temperatures (see Fig. 3(b)).

Nine thermocouples were used to measure the boundary temperatures. The locations of these thermocouples are shown in Fig. 3(b). Note that the temperatures measured by the four thermocouples located at 0.0127 cm from the face were taken to be the temperatures at the surface of the face, and thus provided the face boundary conditions and the radial temperature distribution at the face proper. It should also be emphasized that the radii of 2.01 and 2.63 cm correspond to the inner and outer radii of the seal (rotating) face, respectively. That is, the radial distance spanned by the domain in Fig. 3(b) is equal to the radial distance across the seal face, where the top and bottom boundaries in the figure coincide with the outer and inner radii of the seal face, respectively

EXPERIMENTAL PROCEDURE

As just mentioned, three different sets of temperature measurements were performed during the research, two to justify the use of a two-dimensional computational model and one to obtain the boundary conditions for the model. Each of these sets required a different seat, with each seat having a particular thermocouple deployment. The procedure to obtain these measurements as well as additional temperature measurements will now be detailed.

Prior to performing a particular temperature data set, a number of preparatory steps had to be performed. These steps were common to all of the temperature data sets. First, the thermocouples were cemented in the appropriate holes using copper oxide cement ($k \approx 2.6$ W m^{-1} C^{-1}). Then, the faces of the seat and seal components were lapped flat to within two helium light bands (0.56 μm).

Prior to mounting the seal and seat components, the mounting plate (see Fig. 2(b)), which was mounted on a yolk to facilitate adjustment, was adjusted so that it was perpendicular to the shaft. This was accomplished by securing a dial indicator, with a smallest readable increment of 12.7 μm, to the shaft and positioning the indicator stem so that it was in contact with the face of the mounting plate. Then, the shaft was rotated causing the indicator stem to slide over the face of the mounting plate. When the variation in the reading was within ± 12.7 μm, per revolution, the plate was said to be perpendicular to the shaft.

With the plate so positioned, the lapped seat was pressed into the appropriate counter-bore in the mounting plate. It was then adjusted until its face was perpendicular (to within ± 12.7 μm) to the shaft using the same procedure used to adjust the mounting plate.

The next task to be performed was the mounting of the rotating seal. To begin the mounting process, the rotating seal was inserted into the retainer and positioned so that the eight springs exerted a total force of approximately 200 N on the rear of the seat. Then, the seal was locked into place and subsequently threaded onto the shaft, thus setting the stage for the final adjustment of the rotating face.

To ensure that the eight springs were compressed evenly, and, at the same time, to ensure that the seal face was perpendicular to the shaft (i.e. parallel to the seat face), the dial indicator was fixed to a stationary reference, and the stem was allowed to slide along the seal face while the shaft was rotated. When the variation of the indicator reading was within ± 12.7 μm, the seal face was said to be perpendicular to the shaft, and the springs were said to be evenly compressed (i.e. exerting a uniform force on the rear of the seal). The final spring force was 200 N.

At this point, the test section was assembled, and connected to the flow loop. The test section was then completely insulated using fiberglass insulation ($k \approx 0.049$ W m^{-1} C^{-1}). Then, the gear pump was started; the system pressure was set at 375 kPa absolute; the inlet temperature was set at 30.7°C, and the seal tester was started.

Because of the newly lapped seal and seat components, it was found that the seal and seat ran 'hot' for about the first 20 h of operation. That is, during the first 20 h, the temperatures in the seat consistently ranged from 6 to 8°C, depending upon the shaft speed, above those for times greater than 20 h. Therefore, it was decided to run the tester at the shaft speed corresponding to that characterizing a particular data set for 24 h to 'break in' the newly lapped faces. That is, for the 1500 rpm data set, the seal was broken in at 1500 rpm; for 2500 rpm, break-in was performed at 2500 rpm, etc.

After the 'break-in' period, the seal and seat were allowed to cool to the temperature at the test chamber inlet, thus setting the stage for the data run proper. It was observed during the data runs that after an initial transient, the seat temperatures became steady after about 2 h and were 6–8°C below those for the corresponding shaft speeds during the first 20 h. During the transient, no 'hot spots' were observed. That is, the temperatures were always less than the steady-state values.

During the experiments, each temperature data set was characterized by the particular seat being considered. Recall, a total of three seats, each having a different thermocouple distribution, were used. Each temperature data set consisted of three data subsets, each corresponding to a different shaft speed. In turn, the individual subsets consisted of two separate data runs, with the second being performed to determine the experimental reproducibility.

The execution of a data set began with turning on the seal tester and setting the shaft speed at 1500 rpm and waiting 2 h for the temperatures in the seat and the temperature at the test section exit to reach a steady state. At the end of the 2 h waiting period, the temperatures in the seat were measured using a data logger with a 1 μV resolution and an accuracy of ± 5 counts. All told, five sets of seat temperature readings were recorded at 5 min intervals. These readings were arithmetically averaged to give a single temperature value for each temperature location. The temperatures at the inlet and outlet to the test section were read using a digital multimeter with a 1 μV resolution and an accuracy of ± 2 counts.

After obtaining the first temperature set, the seal tester was stopped, and the seal and seat temperatures were allowed to equilibrate with that of the cooling water. The reproducibility experiment was then performed at the same shaft speed, thus completing the first data subset of the data sets.

The next data subset was performed at 2500 rpm. However, prior to performing the data set, the seal and seat were removed from the tester and relapped. Then, the aforedescribed procedure of adjustment, 'break-in', cool down, seal tester start-up, 2 h waiting period, temperature readings, and replicate data set was repeated. This was also repeated for the 3000 rpm shaft speed.

At the completion of the 3000 rpm data subset, for the experiments performed to establish the thermal boundary conditions to be used in the calculations and for those used to establish the axial temperature gradient, a set of temperature runs were performed with the seat positioned so that the respective thermocouples were 180 deg from the first. That is, the seat was rotated by 180 deg. The entire experimental procedure was then repeated. The arithmetic average of the temperatures, two at each angular position, were used in the finite difference calculations and in the temperature gradient studies.

The exact data taking procedure was used to determine the circumferential temperature distribution, except the seal was not rotated.

COMPUTATIONS AND DATA REDUCTION

In order to determine the heat transfer at the seat face and the Nusselt numbers at the outer radial surface, temperatures were measured along the boundaries of the control volume. The temperature information was used to determine a 'best-fit' temperature distribution for each boundary to create additional data points for the numerical analysis which was used to determine the heat transfer for the seat.

The following heat conduction equation was used to solve for the temperature distribution in the seat:

$$\frac{1}{r}\frac{\partial}{\partial r}\left(k_s r \frac{\partial T}{\partial r}\right)+\frac{1}{r^2}\frac{\partial}{\partial \theta}\left(k_s \frac{\partial T}{\partial \theta}\right)+\frac{\partial}{\partial Z}\left(k_s \frac{\partial T}{\partial Z}\right)=0. \tag{1}$$

Using the measured temperature gradient information, it was found that the θ term in equation (1) was much smaller than the other terms, and it was neglected. Therefore, equation (1) can be written as

$$\frac{1}{r}\frac{\partial}{\partial r}\left(k_s r \frac{\partial T}{\partial r}\right)+\frac{\partial}{\partial Z}\left(k_s \frac{\partial T}{\partial Z}\right)=0 \tag{2}$$

where the thermal conductivity k_s was determined for 304 stainless steel by fitting a least squares line through the data of ref. [8]. The equation is

$$k_s = 0.020T + 14.2 \ (-73^\circ\text{C} \leqslant T \leqslant 127^\circ\text{C}) \tag{3}$$

where T is in °C and k_s has units of W m^{-1} °C^{-1}. The correlation coefficient for the data is 0.996.

Equation (2) was solved by applying the computer program of ref. [9] to the solution domain shown in Fig. 3(b). Figure 4 shows the non-uniform grid spacing used to produce accurate results with minimal computation. Note that in the radial direction, the computational domain (i.e. the region within the circular symbols) spanned the radial distance across the seal face.

Once the temperature distribution was calculated, the axial temperature distributions (i.e. the temperatures denoted by the square symbols in Fig. 4) along the inner and outer radial surfaces of the seat (i.e. at $r = 1.97$ and 2.69 cm) were determined. This was accomplished by curve fitting the r-direction temperatures (i.e. the calculated temperatures between 0.064 and 0.665 cm in Fig. 4) at all of the axial positions and extending the curves out to the respective surfaces. These temperatures were used as the radial boundary conditions for a domain lying between the circular symbols at the z boundaries and the square symbols along the r boundaries in Fig. 4 to recalculate the temperatures within the original domain. Typically, the recalculated temperature field was somewhat different from that which was calculated using the original solution domain between 0.064 and 0.665 cm in Fig. 4. Therefore, the extrapolated surface temperatures had to be adjusted, using a trial and error process, until the recalculated temperature values were within 0.1°C of the original temperature values (i.e. those calculated using the original domain). At this point, the back-calculation process was terminated, and the surface temperatures were considered known. Note that during the back-calculation process, the original radial boundaries (i.e. 0.064 and 0.665 in Fig. 4) were inside of the back-calculation solution domain. It should be emphasized that the main reason for back calculating the axial temperature distributions was to determine the local and average convective heat transfer coefficients along the wetted portion (see Fig. 2(b)) of the outer radial surface of the seat.

The local heat flux distribution at a given surface was obtained by discretizing equation (4)

$$q_n = -k_s \frac{\partial T}{\partial n} \tag{4}$$

where q is the local heat flux and n represents the normal to the desired heat transfer surface. The discretized heat flux equation is

$$q_n = k(T(I))_s \frac{(T(I)-T(I+1))}{\Delta n}. \tag{5}$$

Since the main objective was to determine the local heat flux distribution at the seat face and the local heat transfer coefficients at the outer radial surface, equation (5) was only applied at these surfaces. Therefore, for the seat face, $T(I)$ is the temperature at the face, $T(I+1)$ the temperature at the next node in the z-direction (see Fig. 4) and Δn the distance between the face and the $(I+1)$ node. On the other hand, for the outer radial surface, $T(I+1)$ represents the back-calculated outer radial surface temperature at the locations denoted by the square symbols in Fig. 4 and $T(I)$ the temperature at the preceding node in the r-direction.

It should be mentioned that for the face, equation (5) was applied between $r = 2.03$ and 2.63 cm, while for the outer radial surface, it was applied between $z = 0$ and 0.15 cm.

The local heat transfer coefficients (denoted by h)

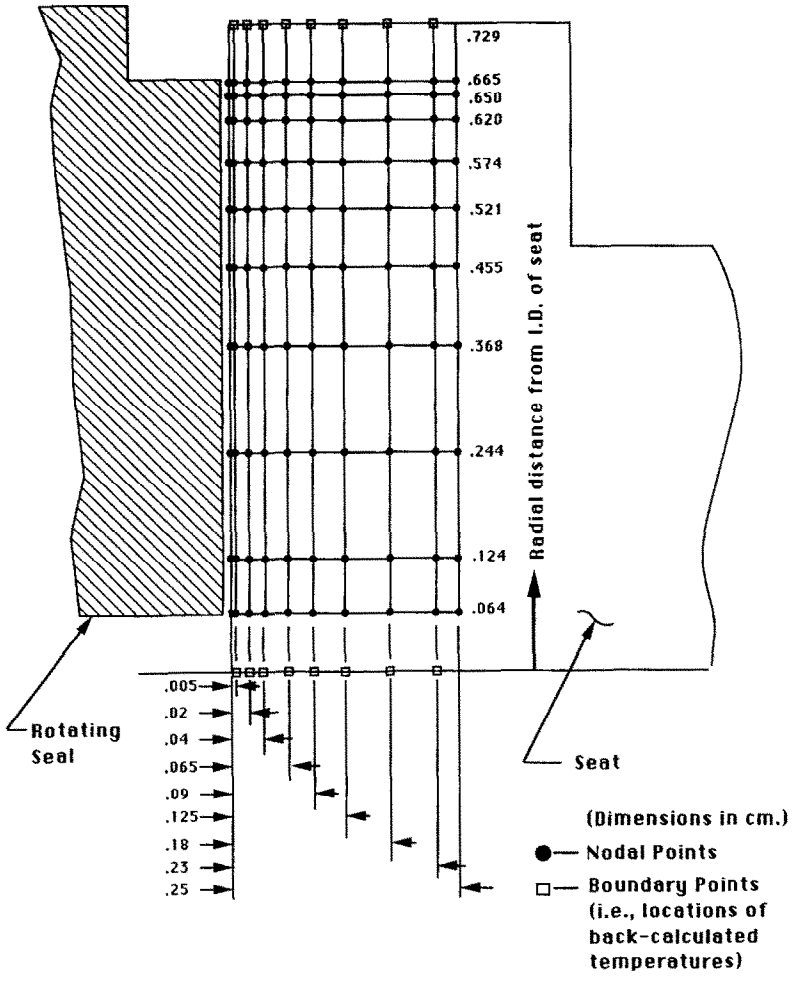

FIG. 4. Non-uniform grid spacing to determine temperature distribution.

along the outer radial boundary of the seat were computed using

$$q_r = h(T_s(z) - T_\infty) \tag{6}$$

where q_r is the local heat flux along the outer radial boundary of the seat computed from equation (5), $T_s(z)$ the temperature of the surface of the seat at a given z location, and T_∞ the temperature of the sealed water given by $(T_{in}+T_{out})/2$ (T_{in} and T_{out} are respectively the temperatures at the inlet and outlet of the test chamber). It should be mentioned that equation (6) is valid for $0 \leqslant z \leqslant 0.15$ cm, that is, for the portion of the outer boundary actually wetted by the sealed water.

From the just calculated local heat transfer coefficients, the local Nusselt numbers for the top boundary were calculated using

$$Nu = hD/k_w \tag{7}$$

where D is the outer diameter of the seat and k_w is the sealed water thermal conductivity evaluated at $(T_s(z)+T_\infty)/2$.

Also of interest was the determination of the average heat transfer for the seat face and outer radial surface. This was accomplished using the following summation:

$$Q_n = \sum_{A_n} q_n \Delta A_n \tag{8}$$

where ΔA_n is an element of surface area normal to the heat flux and A_n the area of the corresponding surface.

The average Nusselt numbers for the outer radial surface were computed using

$$Nu_{AV} = Q_r/A_r\Delta T_{AV}. \tag{9}$$

In equation (9), Q_r is the average heat transfer for the outer radial surface computed from equation (8), A_r the surface area of the portion of the outer radial surface that extends into the sealed water and ΔT_{AV} is an area-weighted average temperature difference given by

$$\Delta T_{AV} = \frac{1}{A_r}\sum_{A_r}(T_s(z) - T_\infty)\Delta A_r \tag{10}$$

where r denotes the outer radial surface.

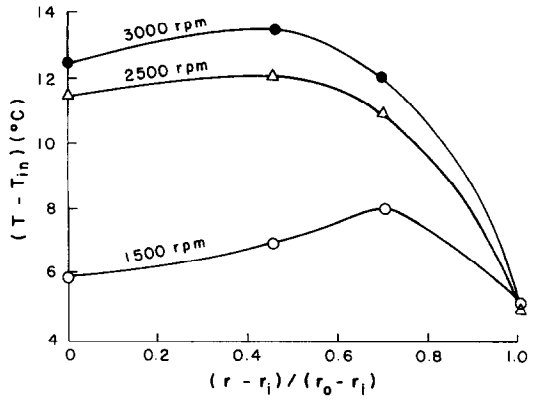

FIG. 5. Seat face temperature profiles at different shaft speeds.

To determine the frictional heat generated at the seal/seat interface, the following relationship was used:

$$Q_{gen} = mc_w(T_{out} - T_{in}) \quad (11)$$

where m is the mass flow rate of water through the test chamber and c_w the constant pressure specific heat of the water at $(T_{out} + T_{in})/2$.

For equation (11) to be valid, the following assumptions need to be valid:

(1) No heat conduction between the seal and the shaft.

(2) No heat conduction through the shaft from the bearing.

(3) No heat generation in the test chamber due to the stirring action.

(4) No heat loss to the ambient.

(5) No heat absorbed by any liquid or vapor that may have leaked past the seal (i.e. negligible leakage).

These assumptions were all validated.

RESULTS AND DISCUSSION

The presentation of results will begin with an examination of the effect of the shaft speed on the temperature behavior of the seat. This will be followed by a presentation and discussion of the heat transfer results.

Temperature results

Figure 5 was prepared to illustrate the effect of the shaft speed on the experimentally measured temperature distribution across the seat face. In the figure, the difference between the seat face temperature and that at the inlet to the test chamber is plotted against the dimensionless radius, $(r-r_i)/(r_o-r_i)$, where r, r_i, and r_o are respectively the radial location of interest, the inner radius of the seal face and the outer radius of the seal face. Recall that the thermocouples at the face of the stationary seat spanned a radial distance that was equal to the distance across the seal face, with the first and last thermocouples positioned at seat locations corresponding to the inner and outer radii of the seal face, respectively (see Fig. 3(b)).

The solid lines connecting the data symbols of similar shape were drawn to provide continuity and to facilitate comparisons between the distributions at the different shaft speeds. It was determined using the uncertainty analysis of ref. [10] that the maximum uncertainty in the temperature differences is $\pm 3\%$.

Before discussing the results in the figure, it should be emphasized that the temperature at the inlet to the test chamber never varied by more than $\pm 0.1°C$ during the research. Therefore, the trends exhibited in Fig. 5 actually portray the behavior of the face temperature. It should also be mentioned that the distributions, corrected for the presence of the inlet temperature, were actually used in the finite difference calculations as the thermal boundary conditions at the seat face.

An examination of the experimental temperature results reveals for the 1500 rpm case that the temperature increases with increasing radius until it reaches its maximum value at a dimensionless radius of about 0.7, with this maximum being about 2.2°C above that at the zero location (i.e. the inner radius of the seal). Beyond 0.7, the temperature drops to its minimum value at a seat location corresponding to the outer radius (the water-wetted side) of the seal, with this drop being about 2.9°C. For 1500 and 2000 rpm shaft speeds, the minimum temperatures in ref. [7], determined from an infra-red pyrometer, also occurred near the radius exposed to the sealed fluid for both water and 10W motor oil.

The temperature distributions for the remaining two shaft speeds are seen to be similar in shape, with these shapes differing appreciably from that at 1500 rpm. It is seen that the highest temperatures occur over the first half (at radii closer to the air side) of the face, with the maximum occurring at about 50% of the way across the face. Beyond the halfway mark, the temperature decays rapidly to its minimum value at the outer radius of the seal, with these drops being 7.0 and 8.3°C for the 2500 and 3000 rpm cases, respectively. The maximum face temperatures computed in ref. [3] for 4000 rpm were also confined to the inner half of the face, but the temperatures increased more rapidly toward the maximum, at the halfway mark, than in this study. As in this study, the temperatures decayed rapidly beyond the halfway point. These results were for the same seal and seat materials that were used for the present work.

In ref. [2], the temperature was measured at seat locations corresponding to the inner and outer radii of the seal for shaft speeds ranging from 1400 to 3000 rpm. It was observed that at all of the shaft speeds considered, the temperature at the inner radius was always 3.5°C above that at the outer radius. The temperature increased with increasing shaft speed, with about a 15°C increase occurring between 1500 and 3000 rpm. This is compared to a 6.8°C increase at the inner radius and essentially no change at the outer

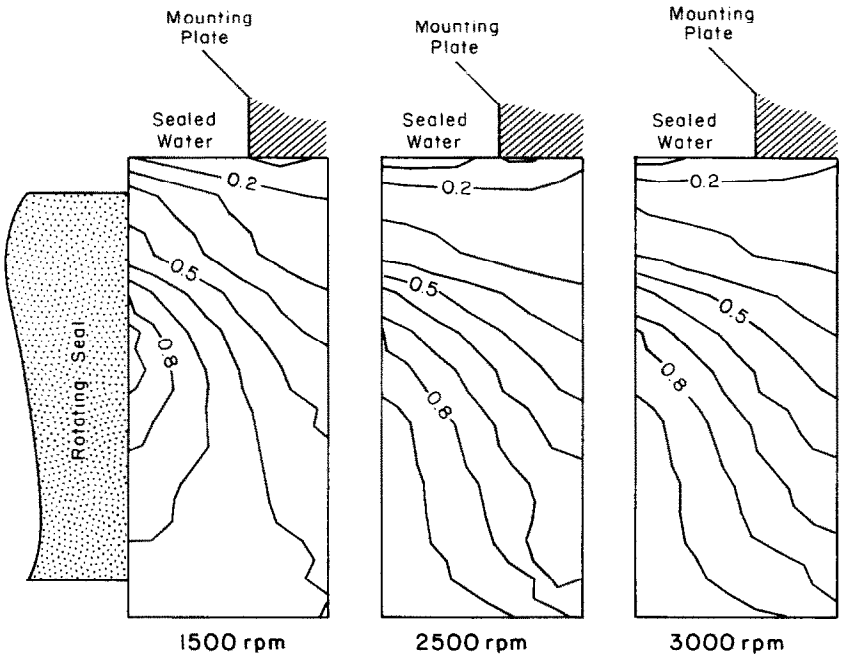

FIG. 6. Cross-sectional seat temperature profiles at different shaft speeds.

radius for the present investigation. The just cited differences may be attributed to the fact that ref. [2] used oil as the sealed fluid as opposed to water for the present study, a Ni-resist-seat-carbon-seal pair opposed to a stainless-steel-seat-carbon-seal pair for the current investigation, and a 75% balance as opposed to a 66% balance for the present work. Reference [3] found that the seal–seat material combination had a significant impact on the seat face temperature levels.

Figure 6 illustrates the effect of shaft speed on the cross-sectional temperature distribution within the seat. The figure consists of three isotherm maps, one for each shaft speed considered. The isotherms in each map have been nondimensionalized using $(T(r,z)-T_{\min})/(T_{\max}-T_{\min})$, where $T(r,z)$ is the temperature at any cross-sectional location and $T_{\min}$ and $T_{\max}$ are respectively the minimum and maximum temperatures in the cross-section. Therefore, the values of the various isotherms range from zero to one.

To ensure clarity, the rotating seal and the portion of the outer radial surface exposed to the sealed water are depicted in the figure. The bottom boundary of each map is exposed to air.

In view of the fact that the direction of heat flow is perpendicular to the isotherms, it is seen for the upper half of the cross-section that the heat flow for the 1500 rpm case moves in a somewhat diagonal direction toward the upper right-hand corner. At the higher shaft speeds, the heat flow in the upper portion of the cross-section is virtually radial. In fact, at the highest shaft speed, the isotherms suggest that the heat that enters axially at the face actually loops backward and exits the top radial boundary with a small negative axial component. The isotherms tend to suggest that the heat transfer coefficients along the wetted top boundary increase with shaft speed. This will be shown to be true shortly.

In the lower portion of the cross-section, it is seen that the axial direction is the preferred direction of heat flow. This is due to low heat transfer coefficients associated with the air that contacts the lower boundary.

Heat transfer results

In Fig. 7, the average heat transfer for the portion of the seat face that coincides with the seal face is plotted as a function of the shaft speed. Since the portion of the total heat generated that is transferred to the seat enters the seat only in the region that coincides with the seal face, the heat transfer results in the figure represent the total heat input to the seat.

When viewing Fig. 7, the data symbols represent the heat transfer calculated from the finite difference scheme (equation (8)). The results in the figure have an uncertainty of $\pm 15\%$. The straight line in the figure is the result of a least squares fit of the individual data points, where the equation of the line is

$$Q_z(\text{watt}) = 0.0115N(\text{rpm}) - 3.40 \qquad (12)$$

where the z subscript refers to the seat face.

The maximum error between the heat transfer represented by the data symbols and that computed from equation (12) is less than 1%.

Figure 8 was prepared to illustrate the effect of the shaft speed on the local heat flux distribution at the seat face. In the figure, the dimensionless heat

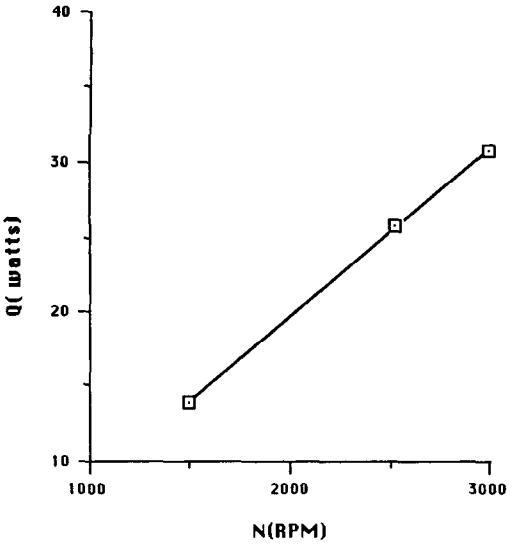

FIG. 7. The effect of shaft speed on the total heat input to the seat.

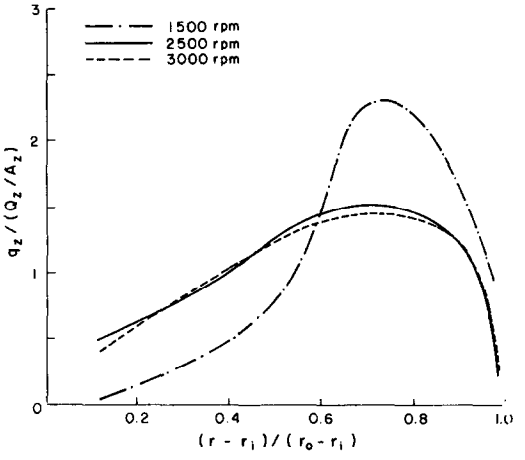

FIG. 8. Seat face heat flux distributions at different shaft speeds.

flux is plotted against the dimensionless radius, which was defined earlier. The heat flux, q_z, was non-dimensionalized by dividing it by Q_z/A_z, where Q_z is the average heat transfer for the seat face from Fig. 7 and A_z is the surface area of the seat face which coincides with the seal face. The uncertainty in the results shown in Fig. 8 are about $\pm 15\%$.

In keeping with the surface temperature results in Fig. 5, an examination of Fig. 8 reveals that the curves for the 2500 and 3000 rpm cases are similar in shape, with these shapes differing from that at the lowest shaft speed. At the lowest shaft speed, the heat flux increases quite rapidly at a non-uniform rate until it attains its maximum value at about 0.75. Beyond this point, the heat flux decays abruptly. For the higher shaft speeds, it is seen that the heat flux initially increases at a much slower and more uniform rate

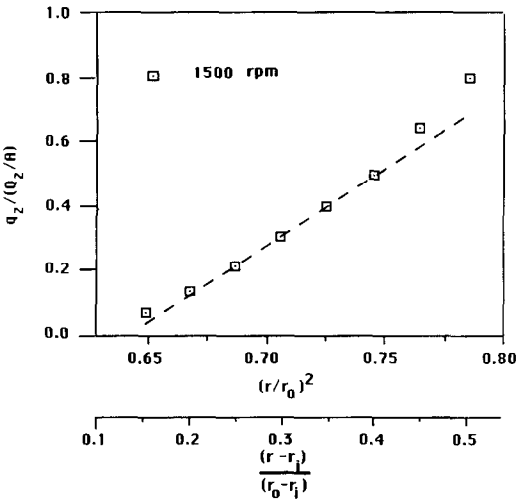

FIG. 9. Linearity of local heat flux for the lowest shaft speed.

than it did at the lowest shaft speed until it reaches a maximum value at a dimensionless radius of about 0.75. Actually, for dimensionless radii between about 0.5 and 0.9, the heat flux remains relatively uniform. After a dimensionless radius of about 0.9, the heat flux drops off dramatically.

The fact that the local face heat flux increases linearly, between dimensionless radii of 0 and about 0.5 for the 2500 rpm shaft speed (to within the uncertainty of the results) and the 3000 rpm shaft speed immediately suggests that the local heat flux is proportional to the local rubbing velocity between the seal and seat faces. Note that for this region, the isotherms in Fig. 6 suggest that the heat flow is nearly axial.

The fact that the heat flux distribution is nearly uniform between dimensionless radii of about 0.5 and 0.9 indicates that the rate of heat removal is increasing at about the same rate as the generation. Note that for this region, the isotherm maps show that the heat flow direction is nearly radial, with the conductive resistance between the wetted boundary decreasing with increasing radius.

A look at the dimensionless heat flux results for the lowest shaft speed shows that a much larger portion of the face heat transfer is concentrated between dimensionless radii of 0.6 and 1.0 than for the higher shaft speeds. The isotherms in Fig. 6 show that the heat flow in this region is less affected by the convection going on at the water-wetted outer boundary than at the higher shaft speeds. This idea will be expanded upon in greater detail later. Note that the region of maximum heat flux corresponds to the region of maximum temperature in Fig. 5 for the lowest shaft speed.

For dimensionless radii between about 0.15 and 0.5, the local heat flux increases much more rapidly with radius at the lowest shaft speed than at the two larger shaft speeds. Figure 9 was prepared to examine the

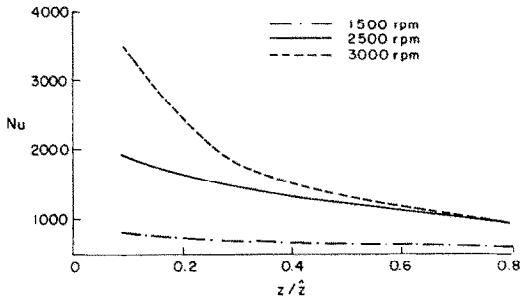

FIG. 10. Local Nusselt numbers at the outer radius of the seat.

behavior in this region in more detail. In the figure, the results (indicated by the symbols) were read off the corresponding curve in Fig. 8 and plotted against $(r/r_o)^2$. The straight line was drawn to emphasize the linearity in the heat flux with radius squared and, the additional scale, $(r-r_i)/(r_o-r_i)$, was drawn to show the range of dimensionless radii over which this behavior occurs. The fact that the heat flux is linear with the radius squared implies that the heat flux is directly proportional to the rubbing velocity squared. Reference [3] based the heat flux levels at the seat face using this assumption.

Attention will now be shifted to the total frictional heat generation. As pointed out earlier, the total heat generation was determined from measurements of the temperatures at the inlet and exit of the test chamber along with the measurement of the mass flow rate through the test section. Recall that the test chamber was engulfed in fiberglass insulation to prevent heat loss to the ambient. Because of the relatively large flow rate of water through the system, it was found that the temperature drop across the test chamber was quite small. This resulted in a very large uncertainty in the heat generation for all of the shaft speeds considered, except the largest shaft speed. Therefore, only the results for the 3000 rpm case will be considered.

It was found that the total heat generation was 3.2 times greater than the total heat absorbed by the seat. Since there was no leakage past the two faces during the experiments, the remaining portion of the total heat generated was absorbed by the seal. Therefore, at 3000 rpm, it was found that the seal absorbed 2.2 times as much of the total heat generated as the seat. This is because the surface area wetted by the sealed water is larger for the seal than the seat, and the corresponding heat transfer coefficients, due to the rotational motion, are believed to be larger for the seal. It should be mentioned that the estimated uncertainty in the total heat generation is $\pm 15\%$. Recall that the uncertainty associated with the heat absorbed by the seat is also $\pm 15\%$.

Attention will now be focused on Fig. 10 and the local Nusselt number distribution across the outer radial boundary, where, in the figure, $\hat{z}$ is the distance (0.15 cm) between the face of the seat and that of the mounting plate and Nu is computed from equation (7). The estimated uncertainty in the results is $\pm 20\%$.

An examination of the figure immediately reveals that, on the whole, the local Nusselt numbers increase with increasing shaft speed, with the most notable increases occurring near the seat face. Since the mass flow rate through the test section was fixed during the experiments, the behavior near the seat face is due to the stirring action of the adjacent rotating seal.

It is seen for the two largest shaft speeds that the local Nusselt number drops off with increasing distance from the face. This is due to the proximity of the mounting plate which acts to damp out the stirring-induced transport mechanisms. Note that the results for the two largest shaft speeds are well within the experimental uncertainty of each other for locations beyond 40% of the way across the wetted surface. As for the lowest shaft speed, it is seen that the local Nusselt numbers are nearly constant.

Table 1 displays the average Nusselt numbers, computed from equation (9), for the outer radial surface of the seat. The reported uncertainties account for computational, temperature measurement, and thermocouple placement errors. These errors were included in all of the uncertainty calculations associated with the computational results of this study. The additional results in the table are included for comparison purposes and will be discussed when appropriate.

In keeping with the local Nusselt results of Fig. 10, the average Nusselt number increases with increasing shaft speed. It is seen that the Nusselt number at the 2500 rpm shaft speed is about a factor of two larger than that at the lowest shaft speed, while the Nusselt number at the highest shaft speed is 23% larger than the value at the 2500 rpm shaft speed.

It is believed that the large increase that occurs between the 1500 and 2500 rpm average Nusselt numbers is the result of turbulence which is being activated at the larger shaft speed. Figure 10 shows that this effect is the most pronounced near the rotating seal face.

Attention will now be directed to the results in the third column of the table. The first three entries in the column are computed using the assumptions of ref. [5] and are calculated for the conditions of the present research. Recall that ref. [5] calculated the average Nusselt numbers for the rotating seal using the standard equations for flow over a flat plate and then assumed that the Nusselt numbers for the seat were equal to those for the seal. The equations used to calculate the first three entries are:

$$Nu_{AV} = 0.664\, Pr^{1/3}\, Re^{1/2} \quad Re \leqslant 5\times 10^5 \text{ (laminar)} \tag{13}$$

and

$$Nu_{AV} = 0.036\, Pr^{1/3}\, Re^{4/5} \quad Re > 5\times 10^5 \text{ (turbulent)} \tag{14}$$

Table 1. Average seat Nusselt numbers

rpm	Nu_{AV} (equation (9))	Nu_{AV}	Percentage difference (%)[a]	Nu_{AV}[b]
1500	640 ± 20%	260 (700) [5]	59 (−9.4)	450 (868)
2500	1300 ± 20%	1050 [5]	19	580 (1300)
3000	1600 ± 20%	1200 [5]	25	670 (1600)
4000		1600 [5] (2000 [3])		770 (2000)

[a] Comparison between equation (9) and ref. [5].
[b] Calculated using equations (13)–(15) using the effective rotating seal diameter as the characteristic length.

where in order to adapt these flat-plate correlations to the cylindrical geometries common in seals, the Nusselt number is based on the circumference rather than the diameter. Therefore, these Nusselt numbers differ from those calculated from equation (7) by a factor of π (i.e. $Nu_{AV} = \pi hD/k_w$).

The Reynolds number is defined as [5]

$$Re = 0.329\frac{R_s^2}{\nu}N \tag{15}$$

where R_s is the outer radius of the seal, N the rotational speed in rpm, and ν the kinematic viscosity at $(T_{sAV}+T_\infty)/2$. It should be pointed out that Re is based on the circumference rather than the diameter, and the velocity is one-half the tangential velocity of the seal at the outer diameter. For this calculation, T_{sAV} is the average temperature of the outer radial surface and is determined by adding T_∞ to ΔT_{AV} in equation (10). The Prandtl number, Pr, is evaluated at the same temperature as the viscosity.

Because of the irregular seal shape used in this work (see Fig. 1), R_s was determined from

$$R_s = \sum_{i=1}^{3} A_i/P_i \tag{16}$$

where i denotes the respective wetted radial surfaces of the seal (see Fig. 1), A_i the surface area of the ith surface, and P_i the circumference. For this case, $R_s = 2.76$ cm.

The Reynolds numbers computed from equation (15) are 4.8×10^5, 8.0×10^5, and 9.6×10^5 for the 1500, 2500, and 3000 rpm cases, respectively. Therefore, equation (14) applies to the two largest shaft speeds and equation (13) applies to the lowest. However, it is believed that turbulence does persist down to the lowest shaft speed. Therefore, it was decided to calculate the Nusselt number for the lowest shaft speed using equation (14), in addition to that using equation (13). The results obtained from equation (14) for the lowest shaft speed are shown in parentheses in Table 1. The fourth column in the table shows the percent difference between the results of this study (equation (9)) and those using the method of ref. [5].

Recall that ref. [5] based the Nusselt and Reynolds number on the circumference rather than the diameter, as in equation (9). In order to compare the results of ref. [5] with those of equation (9), the results of ref. [5] were divided by a factor of π.

Examination of the Nusselt number computed using the technique of ref. [5] shows that the turbulent assumption for the lowest shaft speed holds. The laminar value (equation (13)) of 260 is 59% below the actual value given by equation (9), while the value computed from equation (14), assuming turbulence, is only 9.4% too high, well within the specified uncertainty. A comparison of the remaining results of ref. [5] to those of the current study shows that for the 2500 rpm shaft speed, the result is 19% below the value given by equation (9), which is just within the specified uncertainty. At the 3000 rpm shaft speed, the technique of ref. [5] predicts a value that is outside of the specified uncertainty by 5%.

The entry in the third column corresponding to a 4000 rpm shaft speed ($Re = 12.8\times10^5$) was also computed using the technique of ref. [5]. The value given in parentheses is the value used in the study of ref. [3]. Recall that ref. [3] used the Dittus–Boelter equation to compute the seat Nusselt number. The Reynolds number was based on a representative velocity (4 m s^{-1}) for automobile pumps and a characteristic length equal to twice the annular gap in the pump. The result used by ref. [3] is 25% larger than the value computed using the technique of ref. [5].

Attention will now be focused on the last column in Table 1. These results were also computed using the technique of ref. [5]. However, the Reynolds numbers and Nusselt numbers are based on the seal diameter rather than the seal circumference. The respective Reynolds numbers for the 1500, 2500, and 3000 rpm cases are now a factor of π less. They are: 1.5×10^5, 2.5×10^5, and 3.0×10^5. It is seen that equation (13) is the applicable correlation in all cases. However, since its fairly certain that turbulence does exist, the Nusselt numbers computed from equation (14) are shown in parentheses in the last column.

It is seen that for the 2500 and 3000 rpm cases, the turbulent correlation (equation (14)) gives results that are in perfect agreement with those of equation (9) (the actual results), indicating the replacement of the circumference with the diameter as the characteristic length yields better agreement with the results of this study for the 2500 and 3000 rpm cases. At a 4000 rpm shaft speed ($Re = 4\times10^5$), equation (14) gives a value that is identical to that used by ref. [3].

With regard to the lowest shaft speed, the turbulent value is 36% above the value for the current study,

while the laminar value is 30% below the value of the current work. Furthermore, neither one of these values are as close to the actual value as that computed using the circumference as the characteristic length in equation (14).

CONCLUDING REMARKS

In the present research, experimental measurements were combined with a finite difference technique to study the heat transfer characteristics of a 66% balanced mechanical face seal used to seal water. Temperature distributions and local and average heat transfer results were obtained for the seat for shaft speeds of 1500, 2500, and 3000 rpm. The total amount of heat absorbed by the seal at the largest shaft speed was also determined.

Measured temperature distributions across the seat face and the three remaining boundaries of a two-dimensional computational domain (a portion of the seat cross-section) were used as boundary inputs in a finite difference calculation that yielded the temperature distribution in the domain. This distribution was used to back calculate the temperature across the inner and outer radial surfaces of the seat. The calculated temperature information was used to determine the local heat flux distribution and average heat transfer for the seat face and the local and average Nusselt numbers at the outer radial boundary of the seat.

The axial distributions of the local Nusselt numbers across the water-wetted portion of the seat circumference showed that the local Nusselt numbers were the largest immediately adjacent to the rotating seal, with this value increasing with increasing shaft speed. This behavior was attributed to the stirring action of the rotating seal. It was also seen that the local Nusselt number dropped off with increasing axial distance from the rotating component, with the drop-off being the most dramatic for the maximum shaft speed. Actually, the local Nusselt number was rather constant across the outer circumference of the seat for the lowest shaft speed.

The average Nusselt numbers were also observed to increase with increasing shaft speed, with a 100% increase between the 1500 and 2500 rpm shaft speeds and a 23% increase between the 2500 and 3000 rpm shaft speeds. The large jump in the Nusselt number between the 1500 and 2500 rpm cases was believed to be partially the result of turbulence, which became more active at the larger shaft speeds. It was also found that the average Nusselt numbers for the seat could be accurately predicted for the two largest shaft speeds by setting them equal to those for the rotating seal and using the standard equations for turbulent flow over a flat plate to compute the Nusselt number for the rotating part. This involved computing an effective diameter for the seal and basing the Reynolds number on the effective diameter and a characteristic velocity equal to one half the tangential velocity evaluated at the characteristic diameter. The Nusselt number was also based on the effective diameter.

REFERENCES

1. R. F. Salant and W. E. Key, Development of an analytical model for use in mechanical seal design, 10th Int. Conf. on Fluid Sealing, Innsbruk, Austria, pp. 325–342 (1984).
2. T. G. Doust and A. Parmer, An experimental and theoretical study of pressure and thermal distortions in a mechanical face seal, *ASLE Trans.* **29,** 151–159 (1985).
3. C. H. Li, Thermal deformations in a mechanical face seal, *ASLE Trans.* **19,** 146–152 (1975).
4. G. S. Buck, Heat transfer in mechanical seals, *Proc. 6th Int. Pump Users Symp.*, Texas A&M Univ., College Station, Texas, pp. 9–15 (1989).
5. G. S. Buck, Heat transfer from end face mechanical seals, Report (1977).
6. T. P. Will, Experimental observations of a face-contact mechanical shaft seal operating on water, ASLE/ASME 1981 Lubrication Conf., Preprint 81-FLC-1A-1 (1981).
7. F. K. Orcutt, An investigation of the operation and failure of mechanical face seals, *J. Lubrication Engng* **91,** 713–725 (1969).
8. F. P. Incropera and D. P. DeWitt, *Fundamentals of Heat and Mass Transfer*, 2nd Edn. Wiley, New York (1985).
9. S. V. Patankar, *Numerical Heat Transfer and Fluid Flow*. McGraw-Hill, New York (1980).
10. S. J. Kline and F. A. McClintock, Estimating the uncertainty in single-sample experiments, *Mech. Engng* **75,** 3–8 (1953).

RECHERCHE EXPERIMENTALE ET NUMERIQUE DU TRANSFERT THERMIQUE DANS LES GARNITURES MECANIQUES

Résumé—Des mesures expérimentales sont combinées à des calculs pour obtenir une information sur le transfert thermique local et global à la face du siège d'une garniture mécanique utilisée pour confiner l'eau pour des vitesses de rotation d'arbre de 1500, 2500 et 3000 tr min^{-1}. On obtient les nombres de Nusselt locaux et moyens (à $\pm 20\%$) pour la circonférence mouillée par l'eau. Les nombres de Nusselt moyens pour les deux plus grandes vitesses sont correctement prédits en utilisant les équations classiques de l'écoulement turbulent sur plaque plane pour la portion tournante et en les considérant égaux à ceux pour le siège.

EXPERIMENTE UND BERECHNUNGEN DES WÄRMEÜBERGANGS IN MECHANISCHEN WELLENDICHTUNGEN

Zusammenfassung—Es werden Versuche und Berechnungen ausgeführt, um den örtlichen und mittleren Wärmeübergang an den tragenden Stellen einer mechanischen Wellendichtung gegen Wasser bei Drehzahlen bei 1500, 2500 und 3000 Umdrehungen pro Minute zu ermitteln. Es ergeben sich auch örtliche und mittlere Nusselt-Zahlen (innerhalb $\pm 20\%$) für die wasserbenetzte Umgebung der Dichtfläche. Die mittleren Nusselt-Zahlen bei den beiden größten Drehzahlen lassen sich mit Hilfe der Standardgleichungen für turbulente Strömung an einer ebenen Platte genau berechnen, womit die Bestimmung der Nusselt-Zahlen am rotierenden Teil möglich wird. Es wird schließlich angenommen, daß diejenigen an der Dichtfläche gleich groß sind.

ЭКСПЕРИМЕНТАЛЬНО-ВЫЧИСЛИТЕЛЬНОЕ ИССЛЕДОВАНИЕ ТЕПЛОПЕРЕНОСА В МЕХАНИЧЕСКИХ ТОРЦОВЫХ ГЕРМЕТИЗАТОРАХ

Аннотация—Проводятся экспериментальные исследования и расчеты для определения локальных и средних данных по теплопереносу на наружной поверхности гнезда механического торцового герметизатора для герметизации воды при скоростях вращения вала 1500, 2500 и 3000 об/мин. Получены также локальные и средние числа Нуссельта (с точностью порядка $\pm 20\%$) для охлаждаемой водой круговой поверхности гнезда. С использованием стандартных уравнений, описывающих обтекание плоской пластины турбулентным потоком, точно определены средние числа Нуссельта при двух максимальных значениях скорости вращения вала, позволяющие рассчитать числа Нуссельта для вращающейся части, которые считаются равными значениям для гнезда.